NOVEL STELLARATOR CONFIGURATION WITH DOUBLE HELIX CENTRE POST

P.E. MOROZ
Center for Plasma Theory and Computation,
Department of Engineering Physics,
University of Wisconsin,
Madison, Wisconsin,
United States of America

ABSTRACT. A novel stellarator configuration, the double helix stellarator (DHS), is introduced. It is produced by a double helix centre post and has many unique characteristics. Among them are extreme low plasma aspect ratios, $A \approx 1$, significant rotational transform and extreme-high-β MHD equilibria. Other advantages include a high enclosed volume, absence of noticeable magnetic islands and improved particle transport caused by the absence of a magnetic field ripple on the outboard part of the torus. Compactness, simplicity and modularity of the coil system add to the advantages of the DHS configuration for fusion applications.

1. INTRODUCTION

Very low aspect ratio stellarators represent a fairly new area of research to which not much attention has been paid until very recently, and the lowest aspect ratio stellarators ever built have an aspect ratio, A (which is the ratio of the average major radius, R, to the average minor radius, a, for the last closed flux surface), of about 5. At the same time, a lower aspect ratio and a stronger magnetic field (which is also much easier and less expensive to reach at low aspect ratios) are the main factors in advancing to controlled fusion, as can be explicitly seen from the well known LHD scaling law [1] for the triple product, $nT\tau_E$, accessible in a stellarator,

$$nT\tau_E = 0.045 a^{0.6} R^{-0.2} B_0^{2.4} P^{0.54}. \quad (1)$$

Here, n is the average plasma density in 10^{19} m^{-3}, T is the average plasma temperature in kiloelectronvolts, τ_E is the global energy confinement time in seconds, a and R are in metres, B_0 is the central magnetic field in teslas and P is the total input power in megawatts.

A research programme on very low aspect ratio stellarators, $A \leq 3.5$, with positive plasma current, called spherical stellarators (SSs) in analogy with spherical tokamaks (STs), was proposed in Ref. [2], where the particular configuration with a straight centre post was considered and the advantages of a low aspect ratio for stellarators were discussed. The following main characteristics of an SS are included [2–6] in a definition of this novel class of stellarator configurations:

(a) Very low plasma aspect ratio, $A \leq 3.5$.

(b) High β limits (β is the ratio of plasma pressure to magnetic field pressure), well above the 1 to 5% typical for traditional stellarators.

(c) Positive and substantial plasma current; it is required that in a large and high-β SS device this plasma current be fully supported by the bootstrap effect [4, 5], so there is no need for external current drive.

(d) Improved particle confinement.

Here, positive means that the current flows in a direction such that the rotational transform increases in comparison with its vacuum value, and substantial means that its contribution to the total rotational transform is significant.

More recently, a few other publications [7–16] have appeared on this topic and some other US institutions have become involved in this kind of low aspect ratio stellarator research. Researchers at ORNL focus on J^* transport optimization. They use the name SMARTH (SMall Aspect Ratio Toroidal Hybrid) for the device [12–15]. A different case of SS optimization regarding particle transport can be based on a quasi-axisymmetric approach. The natural tendency of the magnetic structure in some SSs to become more quasi-axisymmetric with increasing plasma current has been stressed before in Ref. [5]. Originally, quasi-axisymmetric stellarators [16, 17] were not considered SS type devices (mainly owing to the larger aspect ratio and no relation to the strong bootstrap current), but more recently the PPPL team [18–20] has used the quasi-axisymmetric approach for transport optimization in an SS type device. The aspect ratio of the configurations presently considered by the ORNL and PPPL teams is in the range $A \approx 2.5$–3.5.

How low can the plasma aspect ratio in a stellarator be? As was mentioned in Ref. [2], in principle, very low aspect ratio stellarator configurations can be obtained simply by reducing the number of twisted (or inclined) toroidal field (TF) coils in the configurations described in Refs [2, 5, 9]. However, this method usually suffers from the disadvantages of low rotational transform and/or strong outboard magnetic ripple, which might have significant negative effects on particle transport and MHD equilibrium and stability characteristics.

In a recent publication [21], a new approach was taken to reducing the aspect ratio in a stellarator further: a new class of stellarators was introduced, extreme low aspect ratio stellarators (ELARSs), and a novel configuration, a single helix stellarator (SHS), with $A \approx 1$, a single toroidal period, vacuum rotational transform $\iota \approx 0.1$–0.15 and advanced confinement characteristics, was considered. To our knowledge, such low aspect ratios have never been considered for stellarators. Moreover, in the spirit of the SS approach, the novel ELARS concept includes the positive plasma current (bootstrap current) as an important element.

The present article can be viewed as a continuation of the research of Ref. [21] on the ELARS configurations, which can be defined roughly as devices with stellarator features and plasma aspect ratios $A < 1.5$. Actually, the aspect ratios of the vacuum configurations in ELARS are even lower, $A < 1.2$. The range of aspect ratios is extended to $A < 1.5$ to include the important cases of high plasma pressure and/or finite plasma current.

Here we consider a different ELARS device, the double helix stellarator (DHS), having vacuum flux surface aspect ratios in the range $A = 1$–1.17 and two toroidal periods, while featuring a number of advanced characteristics regarding particle confinement and extreme-high-β operation. The purpose of the present article is to introduce the novel configuration of the DHS and give an initial demonstration of its advanced characteristics. While an analysis of Ref. [21] was limited to a magnetic field configuration with a single helix post and zero plasma pressure, here we present results for the DHS and also for finite plasma pressure and finite plasma current regimes, which demonstrate clearly significant advantages of ELARS for controlled fusion.

The rest of the article is organized as follows. In Section 2, the coil system of a DHS is presented and the main characteristics of the vacuum magnetic field are described. The results of calculations for finite plasma pressure currentless regimes are given in Section 3. Positive effects of the plasma current are discussed in Section 4, and the advanced neoclassical transport characteristics of the DHS configuration are described in Section 5. Finally, the main conclusions are presented in Section 6.

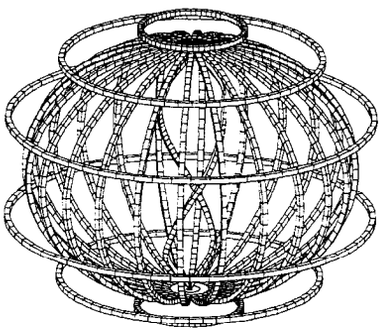

FIG. 1. The DHS coil system.

2. VACUUM MAGNETIC CONFIGURATION OF A DHS

The DHS coil configuration can be obtained from a typical ST coil system by replacing the straight centre post of an ST with a helical post consisting of a double helix, as shown in Fig. 1. The outboard parts of the TF coils can be the same as in an ST and, in principle, can even be replaced by a solid conducting wall (or by many outboard conductors) to reduce the outboard magnetic field ripple. More complicated DHS configurations combining the double helix centre post with the other helical elements of the coil system are possible, but are beyond the scope of the present article.

The configuration presented in Fig. 1 corresponds to the first round of coil system optimization regarding an extreme low aspect ratio, large enclosed volume, large vacuum rotational transform, small outboard magnetic field ripple and small magnetic island structure. The coil system shown includes 24 outboard (half-elliptical) TF coils, 3 pairs of poloidal field (PF) rings, and a centre post consisting of double helix windings making 0.5 turns around the vertical axis.

In principle, the system of closed vacuum flux surfaces can be obtained even without PF rings. The vacuum magnetic field configuration described below in this section corresponds to this case without the PF

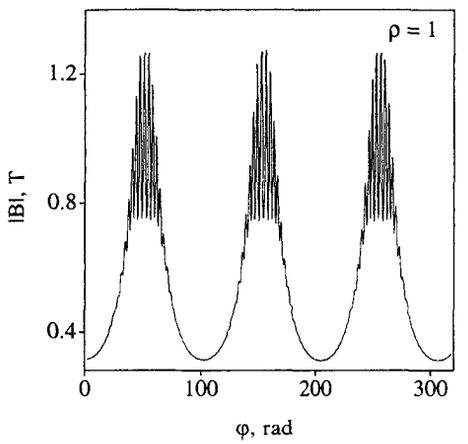

FIG. 2. Variation of $|B|$ along a field line at the LCFS.

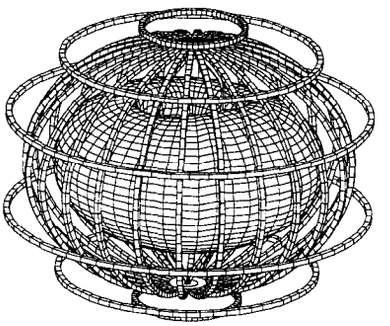

FIG. 3. Perspective view of the LCFS and the DHS coils.

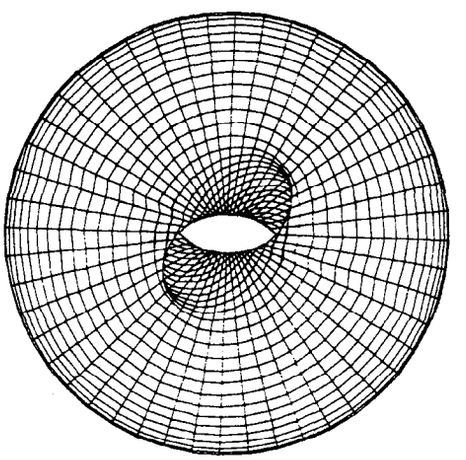

FIG. 4. Plan view on the DHS plasma.

rings. However, the PF rings are very useful for controlling the equilibrium of high-β plasmas, and thus will be used in these cases.

The main reason why we chose a relatively large number (24) of outboard TF coils is because we would like to demonstrate that the outboard magnetic ripple can be almost fully suppressed in the ELARS considered. This situation is very similar to that in a tokamak, where the outboard magnetic ripple can be substantially reduced by increasing the number of TF coils. For a demonstration of this effect, the variation in $|B|$ along the field line for the last closed vacuum flux surface (LCFS) is shown in Fig. 2. This case corresponds to the current $I_h = 600$ kA flowing through each of the two helical elements of the centre post and then returning through the outboard parts of the TF coils. The last flux surface is chosen because it has the largest magnetic ripple. One can see clearly that the magnetic ripple is located practically entirely on the inboard part of the torus and its minima have almost the same level. Later we will return to these questions, as they are important for good particle confinement in the device.

A perspective view of the LCFS and the coils of the ELARS considered is shown in Fig. 3, which demonstrates a significant volume which the plasma can fill within the closed flux surfaces. A plan view of the plasma is shown in Fig. 4. The configuration presented has an aspect ratio of about $A = 1.17$ and an average plasma elongation of $\kappa = 1.3$. All the helical disturbances of the magnetic field and toroidal asymmetries of the configuration are located on the inside of the torus.

Puncture plots for a set of closed vacuum flux surfaces obtained by following along the magnetic field lines are presented in Fig. 5, where the main cross-sections at toroidal angles $\varphi = 0$, $\pi/4$ and $\pi/2$ are shown. A large number of flux surfaces is chosen in Fig. 5 to demonstrate the absence of magnetic islands or stochastic regions within the plasma.

To demonstrate the $|B|$ distribution on flux surfaces, Fig. 6 shows the distribution of $|B|$ over the LCFS. There, B_1 represents the level corresponding to the first solid line, and ΔB is the difference between adjacent contours. The contours with values equal to or above B_1 are shown by solid lines while those with values below B_1 are shown by the dashed lines. This figure clearly demonstrates the peculiarity of the DHS configuration where the quasi-helical symmetry of $|B|$ is maintained in the inboard halves of the flux surfaces while the quasi-toroidal symmetry is typical for the outboard halves. This is exactly opposite to that of the SS configuration of Ref. [2].

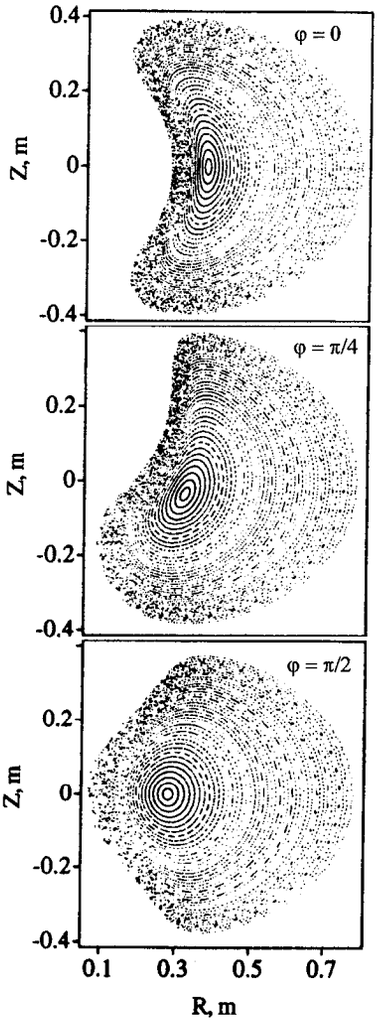

FIG. 5. Poincaré puncture plots for closed vacuum flux surfaces in the main cross-sections, $\varphi = 0$, $\pi/4$ and $\pi/2$.

The vacuum rotational transform in this particular DHS is not very high. It varies from $\iota(0) = 0.095$ to $\iota(1) = 0.063$, as shown in Fig. 7, where $\iota = 1/q$, q being the safety factor. From the point of view of traditional large-A stellarators, these values of ι are small. However, one has to compare not the ι values themselves but rather the ι/A values, having the meaning of the ratio of the average minor plasma radius to the connection length. These values are not smaller for this DHS than for traditional or advanced stellarators such as Wendelstein 7-X [22]. The typical descending character of the radial dependence of ι makes the DHS similar to a tokamak. The addition of a plasma current to a DHS configuration will thus be natural and somewhat analogous to increasing the plasma current in a tokamak.

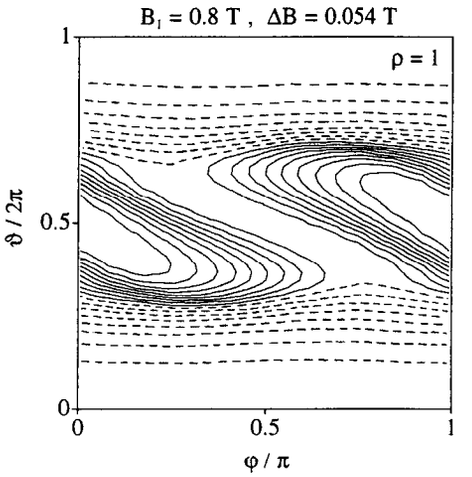

FIG. 6. Distribution of $|B|$ on the LCFS. The solid contours are for $B \geq B_1$ and the dashed contours for $B < B_1$, ΔB is the difference between adjacent contours.

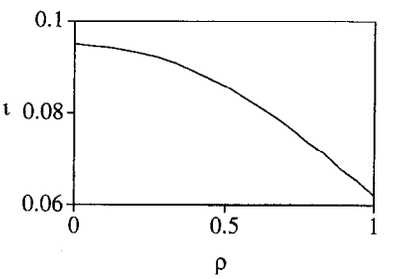

FIG. 7. Vacuum rotational transform.

In this article, we did not try to thoroughly optimize the DHS system, which thus retains a large potential for further optimization. Nevertheless, the DHS configuration considered clearly demonstrates a number of significant advantages and a general potential of this ELARS approach for controlled fusion.

3. FINITE PRESSURE MHD EQUILIBRIA IN A DHS

The vacuum magnetic field configuration of a stellarator corresponds only to a relatively low plasma pressure. For a small experiment, where β cannot be large, this approach is adequate. However, from the point of view of a large machine or, especially, a fusion reactor, the ability of a configuration to confine

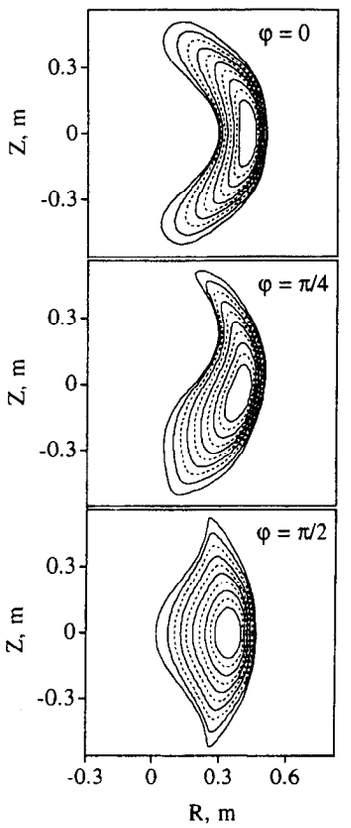

FIG. 8. Three main plasma cross-sections, $\varphi = 0$, $\pi/4$ and $\pi/2$, for the high-β ($\beta_0 = 11\%$, $\beta = 4.5\%$) currentless MHD equilibrium.

the high-β plasmas represents a significant advantage. Internal plasma currents, which may be high at high β, can modify the magnetic configuration significantly. The most important MHD equilibrium effects that might impose limitations on accessible β are the following: the Shafranov shift of the magnetic axis outboard, change of the plasma boundary shape, change of the rotational transform and appearance or growth of the magnetic islands.

In the calculations presented in this article, we are using the three dimensional MHD equilibrium code, VMEC [23], running in the free boundary mode. This code takes into account the actual conductors with the currents. All the above mentioned effects, except the finite-β magnetic islands, can thus be addressed via this code.

There are no reasons to present here the MHD equilibrium cases with low β, as VMEC gives results that are close to those of the vacuum configuration, presented in Section 2. More important is to

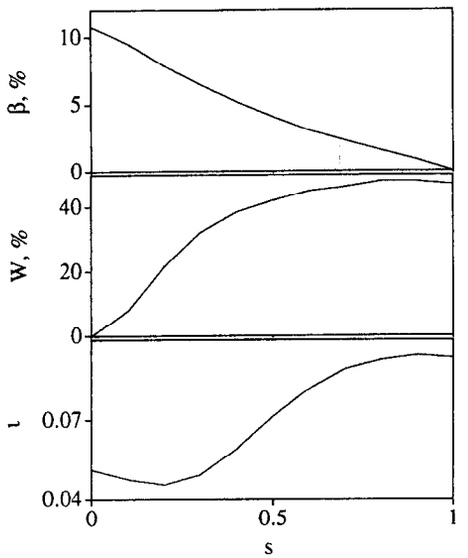

FIG. 9. Radial profiles of β, magnetic well W and rotational transform ι for the high-β currentless case of Fig. 8.

demonstrate the possibility of high-β equilibria. One such case, corresponding to a currentless MHD equilibrium with a central β_0 of 11% and a volume average β of 4.5%, is presented below. These values of β are fairly high and, for comparison, are close to the predicted β limit [24] in the advanced stellarator Wendelstein 7-X.

The main cross-sections, $\varphi = 0$, $\pi/4$ and $\pi/2$, of the flux surfaces are presented in Fig. 8, while the radial profiles of the rotational transform, ι, magnetic well, W, and β values for this equilibrium are shown in Fig. 9. The radial variable, s, is the normalized enclosed toroidal flux. As usual, W is defined through the integral, $U = \int \mathrm{d}l/B$, taken along a field line and averaged over the flux surface,

$$W(\rho) = 1 - \langle U(\rho)\rangle / \langle U(0)\rangle.$$

As one can see, the main high-β effects in a DHS are the following:

(a) Notable Shafranov shift of the magnetic axis outboard;

(b) Decrease of ι in the centre and an increase at the edge, so that the radial profile of ι changes to that of a typical large-A stellarator where ι increases with the minor radius;

(c) Appearance of a significant magnetic well, $W \approx 45\%$ in this case, which is normally of importance for good plasma stability characteristics;

(d) Change of the plasma shape;

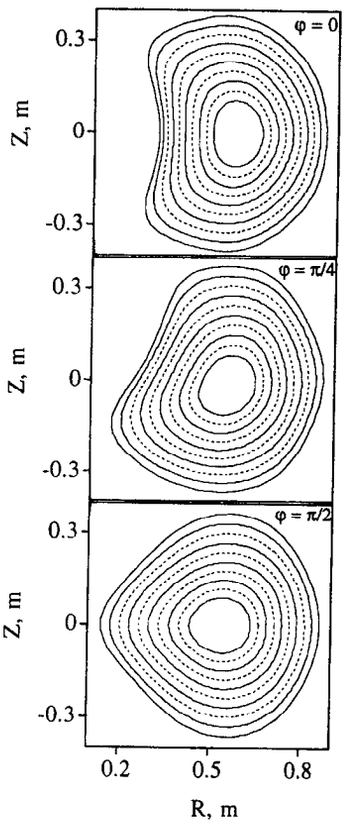

FIG. 10. Three main plasma cross-sections, $\varphi = 0$, $\pi/4$ and $\pi/2$, for the $\beta = 0$, $I_p = 106$ kA MHD equilibrium.

(e) Decrease of the plasma aspect ratio, which becomes slightly below $A = 1$.

The PF rings, which have not been used in the vacuum case, are of importance now, and carry the following currents: $I_{pf1} = 54$ kA (for the rings at $R = 1.05$ m), $I_{pf2} = 13.5$ kA (at $R = 0.75$ m) and $I_{pf3} = 160$ kA (at $R = 0.3$ m).

4. POSITIVE EFFECTS OF THE PLASMA CURRENT

According to the traditional stellarator approach (see, e.g., Refs [22, 24, 25]), a plasma current in a stellarator should be avoided. This includes not only the ohmically driven current but the bootstrap current as well. The absence of a plasma current has often been claimed as one of the main advantages of stellarators.

In contrast, the very positive effects of a plasma current have been identified [4, 5] for the SS configurations, where the ohmically driven current or bootstrap current produce such positive effects as an increase of rotational transform, reduction of particle transport and significant increase of the β limits.

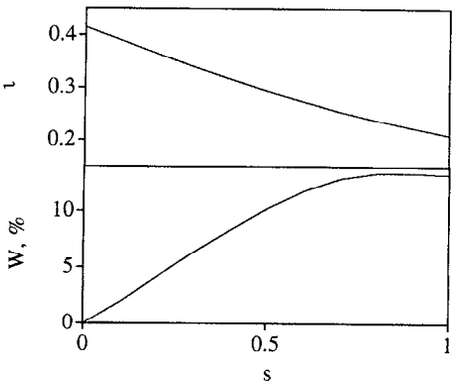

FIG. 11. Radial profiles of ι and W for the current carrying case of Fig. 10.

The bootstrap current is of concern in practically any large stellarator. For example, in LHD, which is under construction at Toki in Japan, it was found [26] that a significant bootstrap current, $I_{bs} > 100$ kA, can already appear at $\beta \sim 1$–2%. However, a stellarator, in principle, can be designed such that the total bootstrap current is positive, negative or close to zero. The latter case corresponds to the standard approach for a stellarator. However, even in this case, it is difficult to fully compensate for the local bootstrap current, which can have positive values at some flux surfaces and negative values at the others. Some stellarators, LHD for example, have auxiliary coils for configuration modification and are flexible enough to study the effects of positive as well as negative bootstrap current. Recent theoretical analysis [27] demonstrated these effects of coil current controls in LHD on configuration properties (such as MHD stability) and bootstrap current.

Here we demonstrate that the plasma current is advantageous for the DHS configurations, similar to that for the above mentioned SS systems. The MHD equilibrium shown in Fig. 10 corresponds to the case of zero plasma pressure and a plasma current of 106 kA, having a parabolic profile. The total rotational transform, ι, and the magnetic well, W, for this equilibrium are given in Fig. 11. Addition of the plasma current in this case introduced the following positive effects: increase of the rotational transform, appearance of a significant magnetic well and decrease of the effective helical ripple, ε_h^{eff}, which dropped to the 1% level at the radial location of half

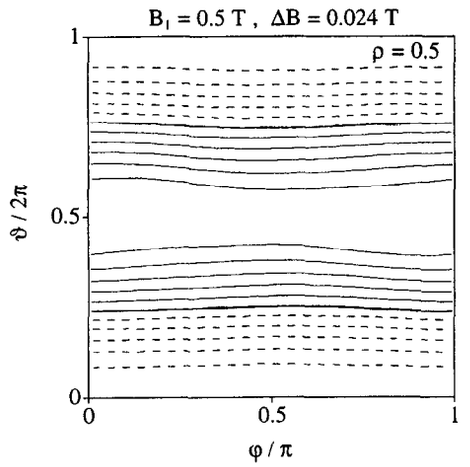

FIG. 12. Distribution of $|B|$ on the $\rho = 0.5$ flux surface for the current carrying case of Fig. 10.

the minor radius, $\rho = 0.5$. The configuration became very close to an axisymmetric one (Fig. 12, where the $|B|$ distribution on the flux surface $\rho = 0.5$ is shown).

The addition of a positive plasma current is of significance in a DHS with high plasma pressure because it has the effect of partially restoring the properties of vacuum flux surfaces: the Shafranov shift decreases and the plasma shape becomes closer to a vacuum one. These effects make possible a further increase of the plasma pressure (correspondingly, the currents in the PF rings should be increased as well). An example of an extreme-high-β MHD equilibrium ($\beta_0 \approx 70\%$, $\beta \approx 30\%$) for this DHS with a plasma current of $I_p = 330$ kA is presented in Fig. 13. The plasma current profile is hollow, which models approximately what will happen with the bootstrap current. The limiting β values for the DHS considered are probably even higher than that just mentioned. The value of the plasma current is such that the total rotational transform is below $\iota = 0.5$ everywhere in the plasma. The radial profiles of β, W, ι and normalized plasma current density, J/J_{max}, for the equilibrium of Fig. 13, are given in Fig. 14.

5. IMPROVED TRANSPORT CHARACTERISTICS OF A DHS

The magnetic field characteristics of stellarators are normally substantially three dimensional. Two known exceptions are represented by the so-called quasi-helically symmetric stellarators [28–31], when

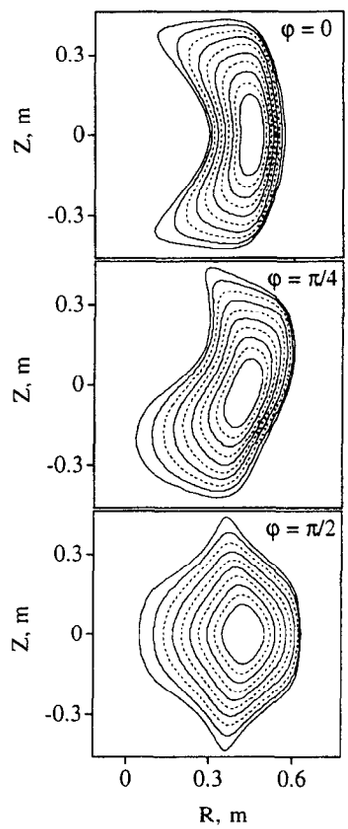

FIG. 13. Three main plasma cross-sections for the extreme-high-β ($\beta_0 \approx 70\%$, $\beta \approx 30\%$) MHD equilibrium with plasma current, $I_p = 330$ kA.

the magnetic field structure in Boozer co-ordinates [32, 33] is close to the helically symmetric one, and the above mentioned quasi-axisymmetric stellarator [16, 17]. These two types of stellarators feature rather good neoclassical transport characteristics. However, quasi-symmetry usually imposes very strict requirements on the configuration, leading to difficulties in obtaining improved high-β characteristics of importance for fusion applications. In addition, there is a difficulty related to the bootstrap current, which is negative in quasi-helically symmetric configurations. This decreases the vacuum rotational transform and can degrade the characteristics of a configuration when β increases. Another difficulty is related to the rather low β limits found so far for quasi-symmetric configurations. The requirements for minimization of the bootstrap current and improvement of the high-β characteristics led the W7-X team [24, 34] to design a stellarator system different from the quasi-symmetric one. In respect to the SS approach, which is very different from the traditional stellarator

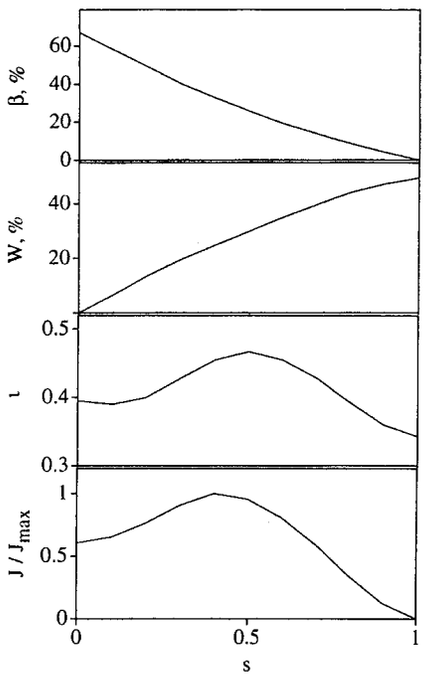

FIG. 14. Radial profiles of β, magnetic well, W, rotational transform, ι, and normalized plasma current density for the extreme-high-β case of Fig. 13.

approach, the quasi-helical symmetry is not accessible, while the quasi-axisymmetry has some chance to succeed although it represents definite limitations for configuration optimization.

Quasi-symmetry is advantageous but not a necessary requirement for improved transport characteristics of a stellarator. Another approach is to find a configuration without a specific symmetry but with improved transport due to the so-called omnigenous particle drifts (i.e. those having guiding centre orbits lying within the same flux surfaces) [35–37]. A set of criteria that can be used for the configuration optimization has also been discussed in Refs [38, 39]. Here, we follow the recommendations [36, 37] to have the magnetic field ripple moved from the outboard to the inboard parts of the flux surfaces. The DHS configuration considered represents a clear example of this approach. Because of this, a DHS is characterized by an improved neoclassical transport.

A simple estimation of the improvement in the low collisional neoclassical transport can be obtained from the S factor [37], which for a general magnetic field of the form

$$B/B_0 = 1 + \sum_{mn} \varepsilon_{mn} \cos(m\theta - nN\varphi) \tag{2}$$

can be written as

$$S = \frac{1}{\rho^2} \int_0^{2\pi} \mathrm{d}\theta\, \varepsilon_{\mathrm{H}}^{3/2} \left[1.778 \left(\frac{\partial \varepsilon_{\mathrm{T}}}{\partial \theta} \right)^2 - 2.133 \left(\frac{\partial \varepsilon_{\mathrm{T}}}{\partial \theta} \right) \left(\frac{\partial \varepsilon_{\mathrm{H}}}{\partial \theta} \right) + 0.684 \left(\frac{\partial \varepsilon_{\mathrm{H}}}{\partial \theta} \right)^2 \right] \tag{3}$$

where

$$\varepsilon_{\mathrm{T}} = \sum_{m \neq 0} \varepsilon_{m0} \cos(m\theta) \tag{4}$$

$$\varepsilon_{\mathrm{H}} = \left[\left(\sum_m \varepsilon_{mn_0} \cos(m\theta) \right)^2 + \left(\sum_m \varepsilon_{mn_0} \sin(m\theta) \right)^2 \right]^{1/2} . \tag{5}$$

To judge how well the configuration is optimized for transport, it is useful to compare the S factor given by Eq. (3) with the factor S_0 calculated for the same configuration but including only the positive definite terms in the square brackets, so that the cancellation caused by the terms with different signs, or enhancement, in the unfavourable case, cannot be realized:

$$S_0 = \frac{1}{\rho^2} \int_0^{2\pi} \mathrm{d}\theta\, \varepsilon_{\mathrm{H}}^{3/2} \times \left[1.778 \left(\frac{\partial \varepsilon_{\mathrm{T}}}{\partial \theta} \right)^2 + 0.684 \left(\frac{\partial \varepsilon_{\mathrm{H}}}{\partial \theta} \right)^2 \right] . \tag{6}$$

The angles θ and φ in the above expressions correspond to the Boozer co-ordinate system, and n_0 corresponds to the main toroidal harmonic number (usually, $n_0 = 1$, which holds also for the DHS configurations considered).

Usually, for low aspect ratio stellarators, which have their magnetic field ripple localized mostly outboard, the parameter $S/S_0 > 1$. For all the DHS configurations considered in this article, this ratio, S/S_0, is lower than 1, and thus the low collisional neoclassical transport is improved. As a demonstration of this, Fig. 15 shows the radial dependence of S/S_0 for all four DHS equilibria considered above: for the vaccum case (circles), for the high-β currentless case (squares), for the current carrying case with $\beta = 0$ (triangles) and for the extreme-high-β equilibrium with plasma current (diamonds).

The ratio S/S_0 (Fig. 15) shows the improvement in particle transport caused by the proper location of

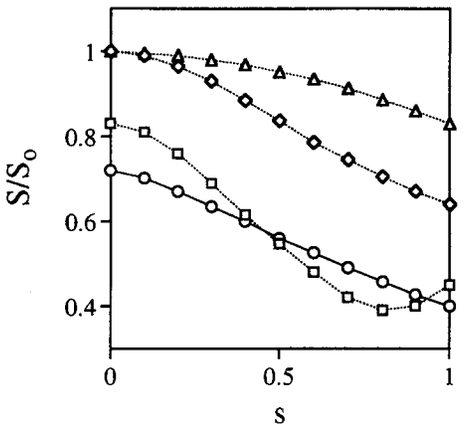

FIG. 15. Radial profiles of S/S_0 for the four equilibria considered: vacuum case (circles), high-β currentless case (squares), current carrying case with $\beta = 0$ (triangles) and extreme-high-β equilibrium with plasma current (diamonds).

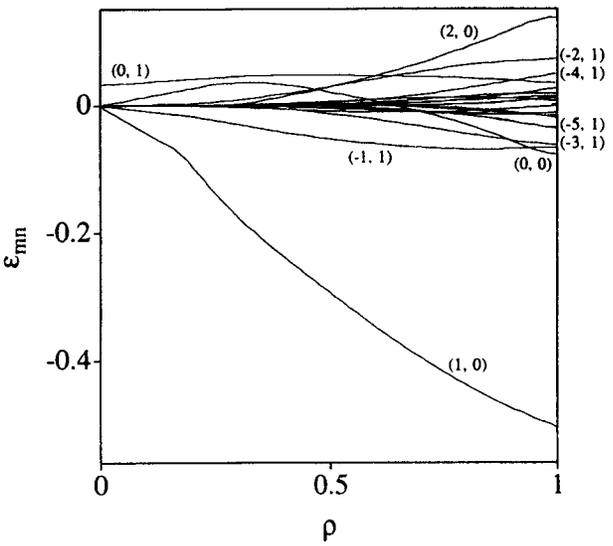

FIG. 16. Magnetic field spectrum for the case of the vacuum DHS configuration.

the helical ripple. This, however, is not a full description as the helical ripple can be large and might, in principle, cause significant ripple transport. The Monte Carlo transport simulations are thus of importance for a full evaluation of the neoclassical transport and for comparison with that in the equivalent tokamak (EQT). We define the EQT to be an axisymmetric device with the same rotational transform as a given stellarator and with its plasma major radius, minor radius and elongation equal to the average corresponding quantities in the given stellarator. The details of the methodology used in the Monte Carlo transport simulations and the results obtained will be presented in a separate publication. Here, we show just a few results for the diffusion coefficient, D_i, for ions (electron ripple transport is smaller), confirming the good transport characteristics in the DHS configurations considered.

The drift motion of the ensemble of K particles, initially distributed arbitrarily along the given flux surface with arbitrary pitch angles but the same kinetic energy, E, has been followed with appropriate pitch angle scattering after each time step. The diffusion coefficient for test particles, D, was defined as

$$D = \frac{a^2}{K} \sum_{k=1}^{K} \frac{[\rho_k(t_k) - \rho(0)]^2}{2t_k} \tag{7}$$

where $\rho(0)$ is the normalized minor radius for the flux surface at which the particles start and $\rho_k(t_k)$ is the normalized minor radius of the particle with index k at time t_k. The ensemble was large enough to ensure a Gaussian distribution of the final particle locations, and the following times, t_k, were larger than the collision time.

The particle transport in a stellarator depends significantly on the spectrum of the magnetic field harmonics, ε_{mn}, in Eq. (2). The corresponding calculations have been carried out for all four DHS cases discussed above. As an example, the Boozer harmonics, ε_{mn}, are shown in Fig. 16 for the case of the vacuum configuration of Fig. 5. The strongest harmonics are labelled with the (m, n) numbers. One can see that the toroidally symmetric harmonics with $n = 0$ are the strongest everywhere except very close to the magnetic axis, where the mirror harmonic (0, 1) is the largest. The strong helical harmonics have $n = 1$, and the harmonics with $n = 2$ have small amplitudes (<2%), even near the plasma edge. All the other harmonics are negligible.

The transition between the low collisionality ripple regime, $\nu^*_\mathrm{st} < 1$, and the plateau regime, $\nu^*_\mathrm{st} > 1$, is defined by

$$\nu^*_\mathrm{st} = \nu/(\varepsilon_\mathrm{h}^\mathrm{eff})^{3/2}\omega_\mathrm{b} \tag{8}$$

where ν is the total collision frequency of a test particle, ω_b is the bounce frequency

$$\omega_\mathrm{b} = \frac{V|n_0 - m_0\iota|}{R} \tag{9}$$

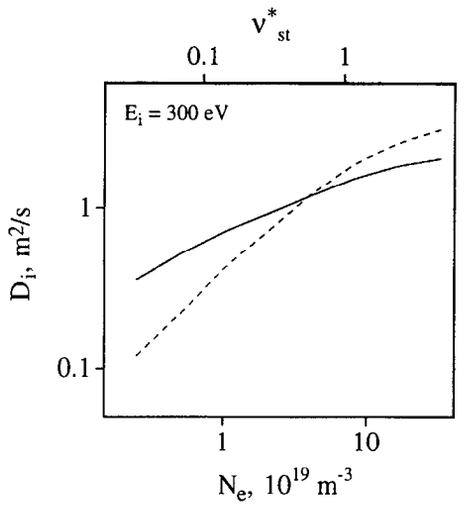

FIG. 17. Ion diffusion coefficient, D_i, for the vacuum DHS configuration (solid curve) and for the corresponding EQT (dashed curve).

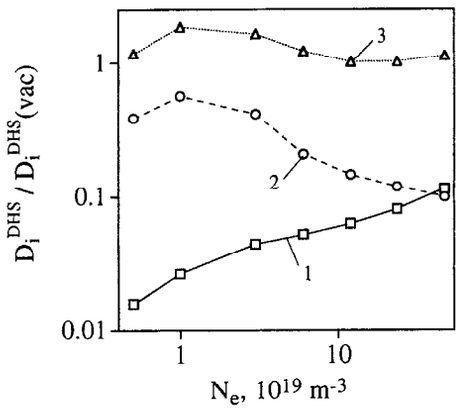

FIG. 18. Ratio D_i/D_i(vac) for three DHS cases, $\beta = 0$, $I_p = 106$ kA (curve 1), $\beta \approx 30\%$, $I_p = 330$ kA (curve 2) and $\beta = 4.5\%$, $I_p = 0$ (curve 3), where D_i(vac) corresponds to the vacuum DHS configuration.

and the effective helical ripple is

$$\varepsilon_h^{eff} = \frac{\pi}{2} \left\langle \left| \sum_{n \neq 0} \varepsilon_{mn} \cos(m\theta - nN\varphi) \right| \right\rangle . \qquad (10)$$

In Eq. (9), $V = \sqrt{2E/M}$ is the velocity of a test particle with mass M, and n_0 and m_0 correspond to the main helical harmonic, which is $(-1, 1)$ for a DHS. In Eq. (10), the angular brackets mean averaging over θ and φ. Below we present the results of calculations of the ion diffusion coefficient at $\rho = 0.5$ for all four DHS configurations discussed. The values of the effective helical ripple at $\rho = 0.5$ for these cases are the following: $\varepsilon_h^{eff} = 0.065$ for the vacuum case of Fig. 5, $\varepsilon_h^{eff} = 0.12$ for the finite-β zero current case of Fig. 8, $\varepsilon_h^{eff} = 0.01$ for the zero-β current carrying case of Fig. 10 and $\varepsilon_h^{eff} = 0.08$ for the extreme-high-β case of Fig. 13.

A comparison of the ion diffusion coefficients, D_i, calculated for the vacuum DHS case of Fig. 5 and for the corresponding EQT is shown in Fig. 17. These calculations were carried out for an ensemble of test protons with energy $E_i = 300$ eV equal to the temperature of the hydrogen background plasma, $T_i = T_e = E_i$. As one can see, the particle confinement in a DHS is close to that in the EQT over a wide range of the collisionality parameter, ν^*_{st}, although it is somewhat higher at very low collisionality. A comparison of D_i for the other three DHS configurations mentioned above with that for the vacuum case is given in Fig. 18. It is important to notice that the diffusion drops significantly for the cases with plasma current (curves 1 and 2 in Fig. 18), which is another indication of the importance of the plasma current in a DHS. For all four DHS configurations considered, our Monte Carlo transport simulations did not show the $D_i \sim 1/\nu$ regime of poor low collisional particle confinement, typical for a standard stellarator. This feature of a DHS can be ascribed to the natural S optimization of the magnetic field in a DHS (there is no magnetic ripple on the outboard part of the torus) and is very advantageous for fusion reactor applications.

6. DISCUSSION AND CONCLUSIONS

A novel stellarator configuration, the DHS, has been introduced. This configuration has a number of features that are unique and very unusual in comparison with those of presently known stellarators. This is an ELARS system. It features extreme low plasma aspect ratios, $A \approx 1$, not known before for stellarators. The DHS is a relative of the SHS configuration recently considered in Ref. [21]. The only helical elements of the DHS configuration considered are the two helical windings replacing the centre post of a standard spherical tokamak coil system. Actually, the DHS features one of the most compact and most spherical plasmas among all the SS configurations [2–11] and satisfies all the SS requirements. Thus, it can be considered a new member of the SS family as well.

In principle, low aspect ratio stellarators are very advantageous for controlled fusion, as shown by the

standard scaling laws [1]. The usual possible difficulty of low aspect ratio stellarators, the unfavorable low collisional neoclassical transport, can be overcome in the DHS configuration, owing to the localization of the magnetic field ripple entirely on the inboard part of the torus. Theoretically, it was shown [36, 37] that such a type of harmonic composition is the most efficient for collisionless plasma confinement. Our calculations of the S factor [37] for different regimes in the DHS configuration confirmed this conclusion. The Monte Carlo simulations of neoclassical diffusion in the DHS configuration demonstrated its good confinement characteristics in all the collisionality regimes. In all the cases considered, the DHS configuration did not show the $1/\nu$ regime of poor confinement at low collisionality so typical of standard stellarators.

The PF rings were not needed, in principle, for the vacuum stellarator configuration to exist. However, they are important at high β (and have been used in our calculations) for plasma control.

Analysis of the currentless regimes with finite plasma pressure in the DHS configuration demonstrated the possibility of high-β MHD equilibria ($\beta = 4.5\%$, $\beta_0 = 11\%$), which also feature good particle transport characteristics. The possibility of accessing high enough β values in the currentless regimes is of importance for the process of plasma startup and heating to the β values where bootstrap current can start to play its positive role.

In contrast to the usual opinion that a plasma current should be avoided in stellarators, our analysis has demonstrated a number of advantages of having a plasma current in a DHS. This is analogous to the positive effects of the plasma current found for the SS configurations [4, 5]. The possibility of extreme-high-β ($\beta_0 \approx 70\%$, $\beta \approx 30\%$) MHD equilibria even with moderate plasma current (such that the total rotational transform is below 0.5 everywhere in the plasma) has been demonstrated.

In this article, we have not touched on a few very important questions that definitely should be investigated before a real machine of this type is constructed. These are the questions of plasma stability and magnetic islands in high-β regimes. There are indications, however, that both these problems can be naturally overcome in a DHS. Regarding the MHD stability, the most dangerous MHD modes, which, in principle, can be unstable in a DHS at high β, are probably the ballooning modes. However, these modes grow on the outboard of the torus where a DHS configuration features toroidal symmetry and is very similar to that of an ST. One can thus suggest that the stability limits in a DHS will be close to those in an ST, which are very high [40]. One can also speculate that the DHS configurations might be naturally stable to high-β magnetic islands because the ι profile has a tendency to become an increasing function of the minor radius (similar to that for the equilibrium of Fig. 8, for example) with increasing plasma pressure (or with the appearance of a bootstrap current). There are preliminary indications [41] that such a profile of ι is advantageous for suppression of the high-β magnetic islands. These positive indications for good stability and suppression of the magnetic islands, however, have to be checked by direct calculations.

Many engineering details, including the forces generated and the supporting structure necessary for the helical centre post, should also be clarified before a DHS can be built. The question of an optimal divertor is also an important element of any fusion relevant machine, especially a compact one such as a DHS. We do not foresee, however, any significant difficulties in resolving these questions beyond those already met by the ST approach. Moreover, we believe that the flexibility of a DHS can help to overcome these difficulties.

There is a significant potential (that we have just started to explore) of the DHS approach for controlled fusion, and further optimization of the DHS coil system will probably result in even higher β regimes with more advanced transport characteristics being found.

While this article was under review, a few new results were obtained and a few relevant presentations [42–45] have been made, which we would like to mention here. The most important new results of these presentations are:

(a) Calculation of the bootstrap current and demonstration of a high-β MHD equilibrium ($\beta_0 = 86\%$, $\beta = 20\%$) accessible with the bootstrap current alone,

(b) Brief consideration of ELARS configurations with single, double and triple helical posts as the members of a family of helical post stellarators (HPSs).

ACKNOWLEDGEMENTS

In conclusion, the author would like to thank S.P. Hirshman for permission to use the MHD equilibrium code, VMEC. The Monte Carlo simulations of

particle transport in a DHS have been carried out via the code written by C.D. Beidler (some modifications to the code have been introduced by J.N. Talmadge and by the author). This work was supported in part by US DOE Grant No. DE-FG02-97ER54395.

REFERENCES

[1] SUDO, S., et al., Nucl. Fusion **30** (1990) 11.
[2] MOROZ, P.E., Phys. Rev. Lett. **77** (1996) 651.
[3] MOROZ, P.E., in Plasma Science (Proc. 23rd IEEE Int. Conf. Boston, 1996), IEEE, New York (1996) 190.
[4] MOROZ, P.E., Phys. Plasmas **3** (1996) 3055.
[5] MOROZ, P.E., et al., Fusion Technol. **30** (1996) 1347.
[6] MOROZ, P.E., Stellarator News **48** (1996) 2.
[7] MOROZ, P.E., et al., Bull. Am. Phys. Soc. **41** (1996) 1567.
[8] MOROZ, P.E., Phys. Lett. A **236** (1997) 79.
[9] MOROZ, P.E., Plasma Phys. Rep. **23** (1997) 502.
[10] MOROZ, P.E., Plasma Phys. Control. Fusion **39** (1997) 1841.
[11] MOROZ, P.E., Nucl. Fusion **37** (1997) 1045.
[12] BATCHELOR, D.B., et al., Bull. Am. Phys. Soc. **41** (1996) 1568.
[13] ROSS, D.W., et al., Plasma Phys. Rep. **23** (1997) 492.
[14] SPONG, D.A., HIRSHMAN, S.P., WHITSON, J.C., Plasma Phys. Rep. **23** (1997) 483.
[15] SPONG, D.A., HIRSHMAN, S.P., WHITSON, J.C., Stellarator News **52** (1997) 1.
[16] GARABEDIAN, P.R., Phys. Plasmas **3** (1996) 2483.
[17] NÜHRENBERG, J., et al., in Theory of Fusion Plasmas (Proc. Joint Varenna–Lausanne Int. Workshop Varenna, 1994) Editrice Compositori, Bologna (1994) 3.
[18] REIMAN, A., et al., Bull. Am. Phys. Soc. **42** (1997) 1913.
[19] ZARNSTORFF, M.C., et al., Bull. Am. Phys. Soc. **42** (1997) 1914.
[20] GOLDSTON, R.J., paper presented at IAEA Tech. Comm. Mtg on Innovative Approaches to Fusion Energy, Pleasanton, 1997.
[21] MOROZ, P.E., Helical post stellarator, Plasma Phys. Control. Fusion (in press).
[22] GRIEGER, G., et al., Phys. Fluids B **4** (1992) 2081.
[23] HIRSHMAN, S.P., RIJ, W.I., MERKEL, P., Comput. Phys. Commun. **43** (1986) 143.
[24] MAASSBERG, H., LOTZ, W., NÜHRENBERG, J., Phys. Fluids B **5** (1993) 3728.
[25] GARABEDIAN, P.R., GARDNER, H.J., Phys. Plasmas **2** (1995) 2020.
[26] WATANABE, K., et al., Nucl. Fusion **32** (1992) 1499.
[27] ICHIGUCHI, K., et al., Nucl. Fusion **37** (1997) 1109.
[28] NÜHRENBERG, J., ZILLE, R., Phys. Lett. **129A** (1988) 113.
[29] GARREN, D.A., BOOZER, A.H., Phys. Fluids B **3** (1991) 2822.
[30] ANDERSON, D.T., et al., Bull. Am. Phys. Soc. **39** (1994) 1601.
[31] BOOZER, A.H., Plasma Phys. Control. Fusion **37** (1995) A103.
[32] BOOZER, A.H., Phys. Fluids **25** (1982) 520.
[33] KUO-PETRAVIC, G., BOOZER, A.H., ROME, J.A., FOWLER, R.H., J. Comput. Phys. **51** (1983) 261.
[34] BEIDLER, C., et al., Fusion Technol. **17** (1990) 148.
[35] HALL, L.S., McNAMARA, B., Phys. Fluids **18** (1975) 552.
[36] MYNICK, H.E., CHU, T.K., BOOZER, A.H., Phys. Rev. Lett. **48** (1982) 322.
[37] SHAING, K.C., HOKIN, S.A., Phys. Fluids **28** (1983) 2136.
[38] CARY, J.R., SHASHARINA, S.G., Phys. Rev. Lett. **78** (1997) 674.
[39] WEITZNER, H., Phys. Plasmas **4** (1997) 575.
[40] MENARD, J.E., et al., Nucl. Fusion **37** (1997) 595.
[41] GOLDSTON, R.J., in Sherwood Fusion Theory Conference (Proc. Conf. Madison, 1997) Paper 2C26.
[42] MOROZ, P.E., paper presented at IAEA Tech. Comm. Mtg on Innovative Approaches to Fusion Energy, Pleasanton, 1997.
[43] MOROZ, P.E., Bull. Am. Phys. Soc. **42** (1997) 1914.
[44] MOROZ, P.E., Phys. Lett. A **243** (1998) 60.
[45] MOROZ, P.E., Bull. Am. Phys. Soc. **42** (1997) 2070.

(Manuscript received 8 September 1997
Final manuscript accepted 25 February 1998)

E-mail address of P.E. Moroz: moroz@engr.wisc.edu

Subject classification: B0, St; C0, St; F2, St